COMMUNICATIONS IN NUMERICAL METHODS IN ENGINEERING
*Commun. Numer. Meth. Engng* 2003; **19**:99–110 (DOI: 10.1002/cnm.573)

# Conjugate filter approach for shock capturing†

Yun Gu[1] and G. W. Wei[1,2,*,‡]

[1]*Department of Computational Science, National University of Singapore, Singapore 117543*
[2]*Department of Mathematics, Michigan State University, East Lansing, MI 28824, U.S.A.*

SUMMARY

This paper introduces a new scheme for the numerical computation involving shock waves. The essence of the scheme is to adaptively implement a conjugate low-pass filter to effectively remove the accumulated numerical errors produced by a set of high-pass filters. The advantages of using such an adaptive algorithm are its controllable accuracy, relatively low cost and easy implementation. Numerical examples in one and two space dimensions are presented to illustrate the proposed scheme. Copyright © 2003 John Wiley & Sons, Ltd.

KEY WORDS: shock capturing; hyperbolic conservation laws; conjugate filters; discrete singular convolution

## 1. INTRODUCTION

A major difficulty in the numerical approximation of non-linear hyperbolic conservation laws is the presence of discontinuities in the solution [1–4]. Traditional schemes generate spurious oscillations in the numerical solution near the discontinuities. The numerically induced oscillations are usually amplified in (time) iterations. Over the last 50 years, a great number of numerical schemes have been proposed for shock capturing. As early as 1950, a solution to this problem was given by von Neumann and Richtmyer [5], who introduced artificial viscosity in a finite difference scheme. This method is simple to use. Unfortunately, the method smears shocks, and serious errors can be induced in the computation of strong shocks. An alternative approach is to construct a full solution by using low-order piecewise discontinuous approximations [6–9]. Such a piecewise solution is a good approximation at the smooth regions, and is capable of representing the shock front over a small region of grid with the use of a Riemann solver. A total variation diminishing (TVD) scheme was proposed by Harten [10] to reduce the spurious oscillations in the numerical solution. The TVD scheme

*Correspondence to: G. W. Wei, Department of Mathematics, Michigan State University, East Lansing, MI 28824, U.S.A
†This paper is dedicated to Professor Chaohui Ye on the occasion of his 60th birthday.
‡E-mail: cscweigw@nus.edu.sg

Contract/grant sponsor: National University of Singapore

*Received 21 August 2001*
*Accepted 6 June 2002*

was later generalized to an essentially non-oscillatory (ENO) scheme [11, 12]. The key idea of the ENO scheme is to use the 'smoothest' stencil among several candidates to approximate the fluxes at cell boundaries to a high-order accuracy and at the same time to avoid spurious oscillations near shocks. This approach was further polished recently in a weighted essentially non-oscillatory (WENO) scheme [13]. Recently, one of the present authors proposed a synchronization-based algorithm for shock computations [14]. A somewhat different approach was proposed by Engquist *et al.* [15]. They applied a non-linear filter of a conservation form at every time iteration to the solution obtained from a standard finite difference scheme.

The existence of so many different approaches for shock capturing indicates both the importance and the difficulty of the problem. The purpose of the present work is to propose a new scheme for shock wave computations. A low-pass filter is introduced to intelligently remove the accumulated numerical errors produced by its conjugate high-pass filters. This set of high- and low-pass filters are conjugate in the sense that they are derived from one generating function and consequently have essentially the same degree of regularity, smoothness, time–frequency localization, effective support and bandwidth. The new approach can reduce the oscillation adaptively without specifically checking the location of the shock wave at each grid point, and thus improve the computational efficiency. In the present study, all conjugate filters are constructed by using a discrete singular convolution (DSC) algorithm [16], which is a potential approach for the numerical implementation of singular convolutions and has controllable accuracy for solving differential equations [16–18].

This paper is organized as follows: Section 2 is devoted to the theory of conjugate DSC filters. A new scheme of treating nonlinear hyperbolic conservation laws is proposed in Section 3. Numerical experiment and conclusion are presented in Sections 4 and 5, respectively.

## 2. CONJUGATE FILTERS GENERATED BY USING DISCRETE SINGULAR CONVOLUTION

The conjugate filters (CFs) are constructed by using the DSC kernels. A brief review of the DSC algorithm is given before CFs are introduced.

Singular convolutions occur commonly in science and engineering. Discrete singular convolution is a potential approach for numerical realization of singular convolutions. The simplest way to introduce the theory of singular convolution is to work in the context of distribution. Let $T$ be a distribution and $\eta(t)$ be an element of the space of test functions. A singular convolution is defined as

$$F(t) = (T * \eta)(t) = \int_{-\infty}^{\infty} T(t-x)\eta(x)\,\mathrm{d}x \tag{1}$$

Here $T(t-x)$ is a singular kernel. Depending on the form of the kernel $T$, the singular convolution is the central issue for a wide range of science and engineering problems. Of particular relevance to the present study are the singular kernels of the delta type

$$T(x) = \delta^{(q)}(x) \quad (q = 0, 1, 2, \ldots) \tag{2}$$

where $\delta$ is the delta distribution. Here the superscript denotes the $q$th-order distribution derivative. The kernel $T(x) = \delta^{(0)}(x)$ is important for the interpolation of surfaces and curves, and

 

$T(x)=\delta^{(q)}(x)$, $(q=1,2,\ldots)$ are essential for numerically solving differential equations. However, distributions cannot be directly implemented for numerical computations. Therefore, it is important to consider a DSC

$$f_\alpha^{(q)}(t)=\sum_k \delta_\alpha^{(q)}(t-x_k)f(x_k) \tag{3}$$

where $f_\alpha^{(q)}(t)$ is an approximation to $f^{(q)}(t)$, $\delta_\alpha(t-x_k)$ is an approximation to the delta distribution and $x_k$ is an appropriate set of discrete points on which the DSC is well defined. It is this approximation that makes a computer realization possible. A variety of DSC kernels $\delta_\alpha(t-x_k)$ have been constructed [16–18]. A simple example is Shannon's kernel

$$\delta_\alpha(x)=(\sin \alpha x)/\pi x \tag{4}$$

Shannon's kernels are of delta sequence and thus provide an approximation to the delta distribution

$$\lim_{\alpha\to\infty}\int \frac{\sin \alpha x}{\pi x}\eta(x)\,\mathrm{d}x=\eta(0) \tag{5}$$

Shannon's kernels have great impact on information theory, signal and image processing because the Fourier transform of Shannon's kernel is an *ideal low-pass filter*. However, the usefulness of Shannon's kernels is limited by the fact that they have a slow-decaying oscillatory tail proportional to $1/x$ in the co-ordinate domain. For signal processing, Shannon's kernels are infinite impulse response (IIR) low-pass filters. Therefore, when truncated by computational applications, their Fourier transforms contain evident oscillations. To improve their behaviour in the co-ordinate representation, a regularization procedure can be used as

$$\delta_{\sigma,\alpha}(x)=\frac{\sin \alpha x}{\pi x}\,\mathrm{e}^{-x^2/2\sigma^2} \quad \sigma>0 \tag{6}$$

Since $\mathrm{e}^{-x^2/2\sigma^2}$ is a Schwartz class function, it makes the regularized kernel applicable to tempered distributions. The regularized kernels can be utilized as finite impulse response (FIR) low-pass filters, since they decay very fast in the co-ordinate domain, and the oscillation in the Fourier domain is dramatically reduced.

For sequences of the delta type, an interpolating algorithm sampling at Nyquist frequency, $\alpha=\pi/\Delta$, has great advantage over a non-interpolating discretization (Here $\Delta$ is the grid spacing). Therefore, on a grid, the regularized Shannon's kernel is discretized as

$$\delta_{\sigma,\pi/\Delta}(x-x_k)=\frac{\sin[(\pi/\Delta)(x-x_k)]}{(\pi/\Delta)(x-x_k)}\,\mathrm{e}^{-(x-x_k)^2/2\sigma^2} \tag{7}$$

The regularized kernel $\delta_{\sigma,\pi/\Delta}(x)$ corresponds to a family of low-pass filter, each with a different compact support, according to $\sigma$ and $\Delta$, in the frequency domain. Its $q$th-order derivative terms are given by analytical differentiations

$$\delta_{\sigma,\pi/\Delta}^{(q)}(x-x_k)=\left(\frac{\mathrm{d}}{\mathrm{d}x}\right)^q\frac{\sin[(\pi/\Delta)(x-x_k)]}{(\pi/\Delta)(x-x_k)}\,\mathrm{e}^{-(x-x_k)^2/2\sigma^2} \tag{8}$$

In this work, $\delta_{\sigma,\pi/\Delta}^{(q)}(x)$ $(q=0,1,2,\ldots)$ are referred as a family of 'conjugate filters'.

 

From the point of view of frequency analysis, the Fourier transforms of $\delta^{(q)}_{\sigma,\pi/\Delta}(x)$ satisfy

$$\hat{\delta}^{(q)}_{\sigma,\pi/\Delta}(\omega) = \mathrm{j}\omega\hat{\delta}^{(q-1)}_{\sigma,\pi/\Delta}(\omega) = (\mathrm{j}\omega)^q\hat{\delta}^{(0)}_{\sigma,\pi/\Delta}(\omega) \tag{9}$$

where $\delta^{(0)}_{\sigma,\pi/\Delta}(x)$ is a symbol for $\delta_{\sigma,\pi/\Delta}(x)$. Since $\hat{\delta}^{(0)}_{\sigma,\pi/\Delta}(0)$ is non-singular,

$$\hat{\delta}^{(0)}_{\sigma,\pi/\Delta}(0) = 1 - \mathrm{erfc}\left(\frac{\pi\sigma}{\sqrt{2}\Delta}\right) \tag{10}$$

where erfc is the error function, it is seen that

$$\hat{\delta}^{(q)}_{\sigma,\pi/\Delta}(0) = 0 \quad (q = 1, 2, \ldots) \tag{11}$$

and thus they are a set of high-pass filters. Due to the common regularizer $\mathrm{e}^{-x^2/2\sigma^2}$, the conjugate filters have essentially the same degree of regularity, smoothness and effective support. In application, the best results are usually obtained if the window size $\sigma$ varies as a function of the central frequency $\pi/\Delta$, such that $r = \sigma/\Delta$ is a parameter chosen in computations. Both interpolation and differentiation are realized by the following convolution algorithm:

$$f^{(q)}(x) \approx \sum_{k=-W}^{W} \delta^{(q)}_{\alpha,\sigma}(x - x_k) f(x_k) \quad (q = 0, 1, 2, \ldots) \tag{12}$$

where $2W + 1$ is the computational bandwidth, or effective kernel support, which is usually smaller than the whole computational domain, $[a, b]$. Note that kernels (12) are either symmetric or antisymmetric, and thus are translationally invariant in the computational domain. Therefore, it is easy to implement. The truncation error is dramatically reduced by the introduction of the delta regularizer. The computational accuracy is controlled by an appropriate choice of $W$.

## 3. CONJUGATE FILTER OSCILLATION REDUCTION ALGORITHM

Figure 1 shows the frequency responses of the conjugate DSC low-pass filter, the first- and second-order high-pass filters at $\sigma = 3.2\Delta$. Indeed, all conjugate filters have essentially the same effective bandwidth, which is about $0.7(\pi/\Delta)$. Below $0.7(\pi/\Delta)$, all the conjugate filters are essentially exact. However, in the very high-frequency region, frequency response of both the low-pass filter and the first-order high-pass filter is under estimating, whereas that of the second-order high-pass filter is over estimating. The proposed idea is to use the conjugate low-pass filter to intelligently eliminate the high-frequency errors produced by the conjugate high-pass filters during the numerical computation. As a consequence, the resulting numerical results are correct and reliable for frequency below the effective bandwidth of the conjugate filters.

Consider a system of nonlinear hyperbolic conservation laws in one dimension (1D)

$$\begin{aligned} u_t + f(u)_x &= 0 \\ u(x, 0) &= u_0(x) \end{aligned} \tag{13}$$

 

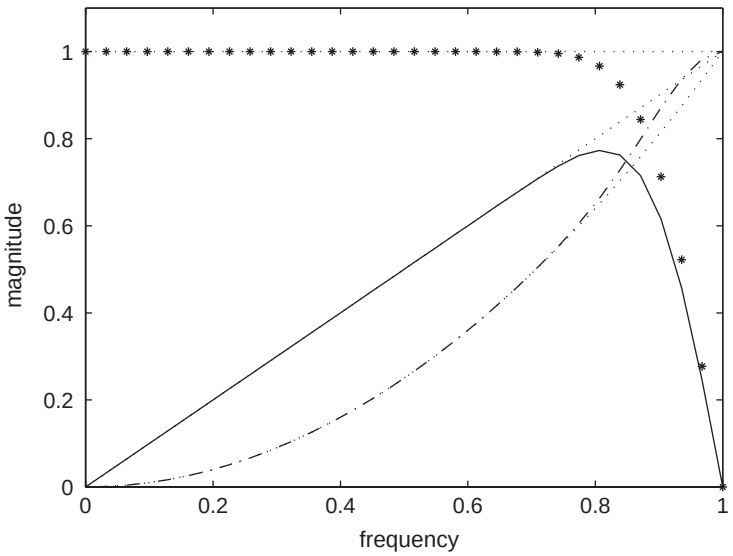


Figure 1. Frequency responses of the conjugate DSC filters (in the unit of $\pi/\Delta$), the maximum amplitude of the filters is normalized to the unit. Stars: conjugate low-pass filter; Solid line: 1st order high-pass filter; Dash-dots: second-order high-pass filter; Small dots: ideal filters.

when $u$ is a vector and $f$ is a hyperbolic mapping. To eliminate spurious oscillations near shocks, we propose the following scheme:

$$v^{n+1} = H(u^n) \tag{14}$$

$$u^{n+1} = \begin{cases} v^{n+1}, & \delta\mathscr{W}^{n+1} < \eta, \\ G(v^{n+1}), & \delta\mathscr{W}^{n+1} \geqslant \eta \end{cases} \tag{15}$$

where $H$ refers to treatment by the DSC high-pass filters, $\delta^{(q)}_{\sigma,\pi/\Delta}$ $(q = 1, 2, \ldots)$ as required by a given problem, and $G$ represents the convolution with the DSC low-pass filter $\delta_{\sigma,\pi/\Delta}$ as given by Equation (12) with $q = 0$. Here $\eta$ is a threshold value, and $\mathscr{W}$ is a high-pass measure, which is defined via a multiscale wavelet transform of a set of discrete function value $\{v(x_k, t_n)\}_{k=1}^{N}$ at time $t_n$ as

$$\|\mathscr{W}^n\| = \sum_m \|\mathscr{W}_m^n\| \tag{16}$$

where $\|\mathscr{W}_m^n\|$ is given by a convolution with a wavelet $\psi_{mj}$ of scale $m$

$$\|\mathscr{W}_m^n\| = \sum_k \left| \sum_j \psi_{mj}(x_k) u^n(x_j) \right| \tag{17}$$

Conjugate low-pass filters are adaptively implemented whenever the difference of high pass measure accesses a positive alarm threshold $\eta$

$$\delta\mathscr{W} = \|\mathscr{W}^{n+1}\| - \|\mathscr{W}^n\| \geqslant \eta \tag{18}$$

 

Table I. Parameters used in the test examples.

| Examples | $r$ | $\eta$ | $\tau$ |
|---|---|---|---|
| 1 | 0.6 | 0.001 | — |
| 2 (Sod) | 0.6 | 0.001 | 0.12 |
| 2 (Lax) | 0.6 | 0.001 | 0.1 |
| 3 | 1.9 | 0.002 | 0.001 |
| 4 | 0.6 | 0.004 | 0.004 |

In the present tests, we use the Haar wavelet of one scale. The choice of $\eta$ depends on the time increment $\Delta t$ and the grid size $\Delta x$.

Since the DSC low-pass filters are interpolative, it is necessary to implement them through prediction $(u(x_k)\rightarrow(x_{k+1/2}))$ and restoration $(u(x_{k+1/2})\rightarrow u(x_k))$. For non-linear hyperbolic systems, the use of an additional filtering at a regular time interval $\tau$ gives a better results. The conjugate filters are non-linear in space-time. The use of such adaptive filters is cost efficient and simple to implement. A standard fourth-order Runge–Kutta scheme is used for the time integration. It is very easy to extend the conjugate filters to higher-order space dimensions.

## 4. NUMERICAL EXPERIMENTS

In this section, a few benchmark numerical problems, including a wave equation, 1D and 2D Euler systems, are employed to test the proposed scheme and to demonstrate its utility. We choose $W=32$ in all the computations. The parameter of $r=3.2$ is used for high-pass filters and for the low-pass filter prediction. For nonlinear examples, we also apply the low-pass filter at a fixed time interval $\tau$. The parameters $\tau$, $\eta$ and $r$ for the restoration are summarized in Table I for all experiments.

*Example 1*
Consider a linear equation

$$\begin{aligned} u_t + u_x &= 0, \quad -1<x<1 \\ u(x,0) &= u_0(x), \quad u_0(x) \text{ periodic with period } 2 \end{aligned} \tag{19}$$

Three sets of initial data $u_0(x)$ are used. The first one is $u_0(x)=\sin(\pi x)$. The errors of the proposed scheme at time $t=1$ are listed in Table II, and compared with those of the

Table II. Comparison of errors of two shock capturing schemes.

| | $L_1$ errors | | $L_\infty$ errors | |
|---|---|---|---|---|
| $N$ | DSC | WENO-RF-5 | DSC | WENO-RF-5 |
| 10 | 5.09(−09) | 1.60(−02) | 5.00(−09) | 2.98(−02) |
| 20 | 4.24(−14) | 7.41(−04) | 2.23(−13) | 1.45(−03) |
| 40 | 5.28(−16) | 2.22(−05) | 5.42(−15) | 4.58(−05) |

 

Table III. Comparison of errors of two shock capturing schemes.

| | $L_1$ errors | | $L_\infty$ errors | |
|---|---|---|---|---|
| $N$ | DSC | WENO-RF-5 | DSC | WENO-RF-5 |
| 20 | 4.12(−10) | 4.91(−02) | 1.00(−09) | 1.08(−01) |
| 40 | 1.11(−16) | 3.64(−03) | 2.07(−15) | 8.90(−03) |
| 80 | 3.44(−17) | 5.00(−04) | 8.23(−16) | 1.80(−03) |

WENO-RF-5 scheme [13]. Here $N$ is the total number of cells, and $\Delta t/\Delta x$ is optimized. It is seen that the proposed scheme yields a very high accuracy even for a very few number of cells ($N = 10$).

The next case is given by $u_0(x) = \sin^4(\pi x)$. The errors at time $t = 1$ are listed in Table III for two different schemes. The proposed scheme attains high accuracy.

The third initial value is given by [13]

$$u_0(x) = \begin{cases} \frac{1}{6}[D(x,\beta,z-\delta) + D(x,\beta,z+\delta) + 4D(x,\beta,z)], & -0.8 \leqslant x \leqslant -0.6; \\ 1, & -0.4 \leqslant x \leqslant -0.2; \\ 1 - |10(x-0.1)|, & 0 \leqslant x \leqslant 0.2; \\ \frac{1}{6}[F(x,\alpha,a-\delta) + F(x,\alpha,a+\delta) + 4F(x,\alpha,a)], & 0.4 \leqslant x \leqslant 0.6; \\ 0, & \text{otherwise} \end{cases}$$

where functions $D$ and $F$ are given by

$$D(x,\beta,z) = \mathrm{e}^{\beta(x-z)^2}$$

$$F(x,\alpha,a) = \sqrt{\max(1-\alpha^2(x-a)^2, 0)}$$

Here the constants are taken as $a = 0.5$, $z = -0.7$, $\delta = 0.005$, $\alpha = 10$ and $\beta = \log 2/(36\delta^2)$. The solution contains a smooth but narrow combination of a Gaussian, a square wave, a sharp triangle wave, and a half-ellipse. This is a case with the so-called *contact discontinuities* and is quite difficult to handle in hyperbolic systems.

Equation (13) is integrated up to $t = 8$ with 201 grid points in the domain of $[-1, 1]$. The numerical results are shown in Figure 2. It is observed that the new scheme has a good performance. These results are some of the best available to date for the problem.

*Example 2*

To further test the proposed scheme, we consider the 1D Euler equations of gas dynamics. The governing equations take the form

$$\begin{bmatrix} \rho \\ \rho u \\ E \end{bmatrix}_t + \begin{bmatrix} \rho u \\ \rho u^2 + p \\ u(E+p) \end{bmatrix}_x = \mathbf{0} \tag{20}$$

 

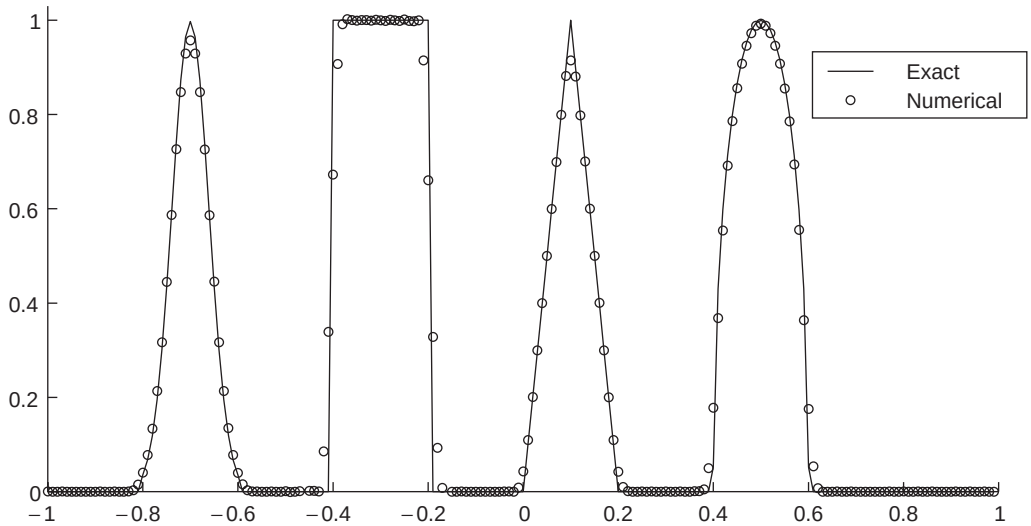


Figure 2. Linear equation. $t = 8$, $\Delta x = 0.01$ and $\Delta t/\Delta x = 0.1$.

where $\rho$ is the density, $u$ the velocity, $E$ the total energy, $\gamma = 1.4$ a constant and $p$ the pressure which is given by

$$p = (\gamma - 1)(E - \tfrac{1}{2}\rho u^2) \tag{21}$$

Two well-known Riemann problems, Sod's problem and the Lax problem, are employed. The initial data of Sod's problem [13] are

$$\rho = 1, \quad u = 0, \quad p = 1, \text{ when } x < 0$$
$$\rho = 0.125, \quad u = 0, \quad p = 0.1, \text{ when } x \geqslant 0$$

The numerical result of density at $t = 2.0$ is shown in Figure 3(a).

The other set of data was given by Lax [19]

$$\rho = 0.445, \quad u = 0.698, \quad p = 3.528 \quad \text{when } x < 0$$
$$\rho = 0.5, \quad u = 0, \quad p = 0.571 \quad \text{when } x \geqslant 0$$

The numerical result of density at $t = 1.5$ is shown in Figure 3(b).

It is seen that the proposed scheme gives a correct solution with good resolutions for both problems. Except for the contact discontinuity, the shock fronts are well preserved.

*Example 3*

We next consider the problem of shock entropy wave interactions [13]. In this problem, the interaction of an entropy wave of small amplitude with a moving shock in a 1D flow is

 

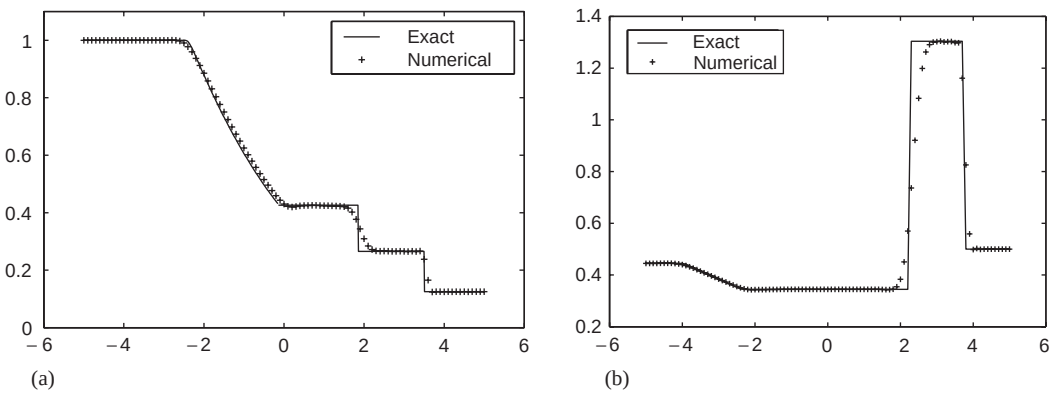


Figure 3. Riemann problems of the Euler system (density): (a) Sod problem: $t = 2.0$, $\Delta x = 0.1$, $\Delta t/\Delta x = 0.2$; and (b) Lax problem: $t = 1.5$, $\Delta x = 0.1$, $\Delta t/\Delta x = 0.2$.

numerically investigated. The governing equations are the same as those of Example 2. On the interval $[0, 5]$, the initial values are

$$\rho = 3.85714, \quad u = 2.629369, \quad p = 10.33333 \quad \text{when } x < 0.5$$

$$\rho = \mathrm{e}^{-\varepsilon \sin(kx)}, \quad u = 0, \quad p = 1 \quad \text{when } x \geqslant 0.5$$

where $\varepsilon$ and $k$ are the amplitude and wave number of the entropy wave, respectively [13]. The mean flow is a pure right-moving Mach 3 shock.

The goal of this test is to examine the stability and accuracy of the new scheme in the presence of the shock. Since the entropy wave is set to be very weak compared to the shock, any excessive oscillation might pollute the generated sound waves and the amplified entropy waves. We take $\varepsilon = 0.01$ and $k = 13$ in our test. The amplitude of the amplified entropy waves predicted by the linear analysis is 0.08690716. This is a numerically challenging case. Low-order schemes will dramatically damp the magnitude of the transmitted wave. In our test, 800 grid points are used to resolve the passing waves. The numerical results are shown in Figure 4. The only amplitude of the entropy wave component is displayed. The mean flow and the generated sound waves (or pressure wave), which are of lower frequency than the amplified entropy waves and thus are much better resolved by this grid size, have been subtracted from the numerical solution. It is seen that the proposed scheme performs well with respect to the prediction of the amplified entropy waves at higher frequency downstream of the shock. The amplified entropy waves are fully resolved. The present results are some of the best available for this problem to our knowledge. The advantage of the proposed high order approach over previous schemes is apparent.

*Example 4*

We finally test the proposed scheme by using the 2D problem of 'a Mach 3 wind tunnel with a step'. The problem is a standard test case for high-order scheme [8]. The governing

 

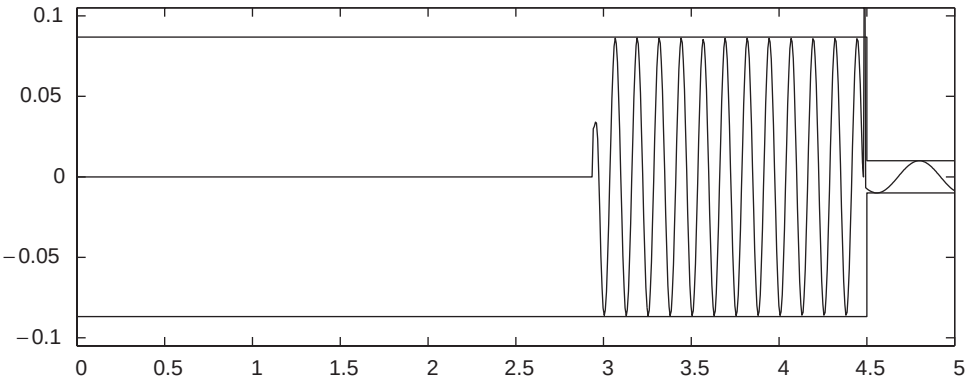


Figure 4. 1D shock entropy wave interaction: the amplitude of entropy waves; $N = 800$, $\Delta t = 0.001$.

equations take the form

$$\begin{bmatrix} \rho \\ \rho u \\ \rho v \\ E \end{bmatrix}_t + \begin{bmatrix} \rho u \\ \rho u^2 + p \\ \rho uv \\ u(E+p) \end{bmatrix}_x + \begin{bmatrix} \rho v \\ \rho uv \\ \rho v^2 + p \\ v(E+p) \end{bmatrix}_y = \mathbf{0} \tag{22}$$

where $(u, v)$ is the 2D fluid velocity and $p$ is given by

$$p = (\gamma - 1)(E - \tfrac{1}{2}\rho(v^2 + u^2)) \tag{23}$$

The tunnel begins with a uniform Mach 3 wind flow which encounters a step. The width and length of the wind tunnel are 1 and 3 length units, respectively. The step is 0.2 length units high and is located 0.6 length units from the left-hand end of the tunnel. The tunnel is assumed to have an infinite width in the direction orthogonal to the plane of the computation. At the left is a flow-in boundary condition, and at the right all gradients are assumed to vanish. The exit boundary condition has no effect on the flow, because the exit velocity is always supersonic. Initially the wind tunnel is filled with a gamma-law gas, with $\gamma = 1.4$, in which everywhere has density 1.4, pressure 1.0, and velocity 3. Gas with this density, pressure, and velocity is continually fed in from the left-hand boundary.

Along the walls of the tunnel reflecting boundary conditions are applied. The corner of the step is the center of a rarefaction fan and hence is a singular point of the flow. Without special treatment of the singularity, the flows are seriously affected by large numerical errors generated just in the neighbourhood of this singular point. These errors cause a boundary layer of about one zone in thickness to form just above the step in the wind tunnel. Shocks then interact with this boundary layer, and the qualitative nature of the flow in the tunnel is altered more or less dramatically, depending upon different schemes. For the treatment of the singularity at the corner of the step, we adopt the technique used in Reference [8].

In Figure 5, the contours of density obtained on the grid $\Delta x = 1/80$ at $t = 4$ is shown. Our new scheme achieves very fine resolution and contains very few visible 'bumps', which, in fact, are small numerical oscillations. Also note that the effects of the numerical boundary

 

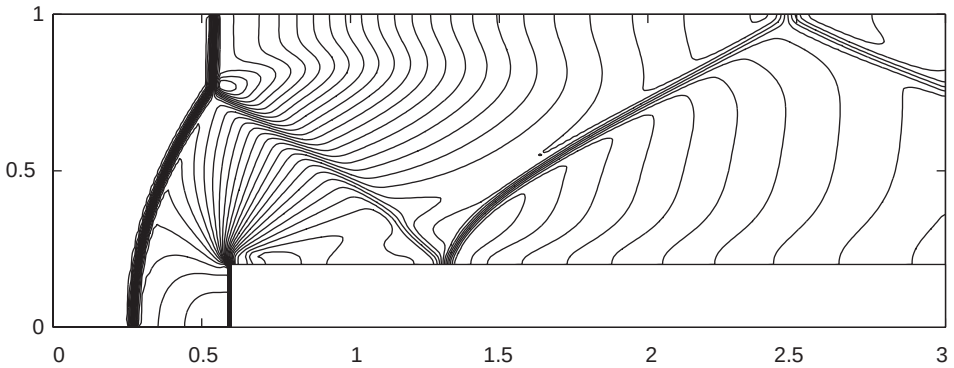


Figure 5. A Mach 3 flow past a wind tunnel with a step. $\Delta t = 0.001$, $\Delta x = 1/80$ and $t = 4.0$. In the plot 30 equally spaced contours of density are shown.

layer along the top of the step in the duct are very weak. The weak shock from the corner of the step is resolved.

## 5. CONCLUSION

In conclusion, a novel approach is introduced for solving the problem of non-linear hyperbolic conservation laws. The essence of the new scheme is to adaptively implement a conjugate low-pass filter to effectively remove the accumulated numerical errors produced by a set of high-pass filters. The conjugate low-pass and high-pass filters are derived from a single function and thus, have essentially the same degree of regularity, smoothness, time–frequency localization, effective support and bandwidth. In this work, all conjugate filters are constructed by using discrete singular convolution kernels, which have controllable accuracy for numerical simulations. Numerical experiments indicate that the new scheme is efficient, and reliable. Further work on the parameter selection of the proposed scheme is under consideration.

ACKNOWLEDGEMENT

This work was supported by the National University of Singapore.

REFERENCES

1. Balaguer A, Conde C, Lopez JA, Martinez V. A finite volume method with a modified ENO scheme using a Hermite interpolation to solve advection–diffusion equation. *International Journal for Numerical Methods in Engineering* 2001; **50**:2339–2371.
2. Wong GCK, Wong SC. A wavelet-Galerkin method for the kinematic wave model of traffic flow. *Communications in Numerical Methods in Engineering* 2000; **16**:121–131.
3. Bertolazzi E. A finite volume scheme for two-dimensional chemically reactive hypersonic flow. *International Journal of Numerical Methods in Heat Fluid Flow* 1998; **8**:888.
4. Baumann CE, Storti MA, Idelsohn SR. Improving the convergence rate of the Petrov–Galerkin techniques for the solution of transonic and supersonic flows. *International Journal for Numerical Methods in Engineering* 1992; **34**:543–568.
5. von Neumann J, Richtmyer RD. A method for the numerical calculation of hydrodynamic shocks. *Journal of Applied Physics* 1950; **21**:232–237.

 

6. Godunov SK. Finite difference method for numerical computation of discontinuous solutions to the equations of fluid dynamics. *Mathematicheski Sbornik* 1959; **47**:271.
7. van Leer B. Towards the ultimate conservative difference scheme. IV. A new approach to numerical convection. *Journal of Computational Physics* 1977; **23**:276.
8. Woodward PR, Colella P. The numerical simulation of two-dimensional fluid flow with strong shocks. *Journal of Computational Physics* 1984; **54**:115–173.
9. Bell JB, Colella P, Glaz HM. A second-order projection method for the incompressible Navier–Stokes equations. *Journal of Computational Physics* 1989; **85**:257–283.
10. Harten A. High resolution schemes for hyperbolic conservation law. *Journal of Computational Physics* 1983; **49**:357–393.
11. Harten A, Engquist B, Osher S, Chakravarthy S. Uniform high-order accurate essentially non-oscillatory schemes III. *Journal of Computational Physics* 1987; **71**:231–303.
12. Shu C-W, Osher S. Efficient implementation of non-oscillatory shock capturing schemes. *Journal of Computational Physics* 1988; **77**:439–471.
13. Jiang G-S, Shu C-W. Efficient implementation of weighted ENO schemes. *Journal of Computational Physics* 1996; **126**:202–228.
14. Wei GW. Synchronization of single-side averaged coupling and its application to shock capturing. *Physics Review Letters* 2001; **86**:3542–3545.
15. Engquist B, Lötstedt P, Sjögreen B. Nonlinear filters for efficient shock computation. *Mathematics of Computation* 1989; **52**:509–537.
16. Wei GW. Discrete singular convolution for the solution of the Fokker–Planck equations. *Journal of Chemical Physics* 1999; **110**:8930–8942.
17. Wei GW, Zhao YB, Xiang Y. Discrete singular convolution and its application to the analysis of plates with internal supports. I Theory and algorithm. *International Journal for Numerical Methods in Engineering* 2002; **55**:947–972.
18. Wei GW. A new algorithm for solving some mechanical problems. *Computer Methods in Applied Mechanics and Engineering* 2001; **190**:2017–2030.
19. Lax PD, Wendroff B. Systems of conservation laws. *Communications on Pure and Applied Mathematics* 1960; **13**:217–237.

 